Hindawi
Shock and Vibration
Volume 2019, Article ID 4358631, 14 pages
https://doi.org/10.1155/2019/4358631

Research Article

Stability Analysis of a Nonlinear Coupled Vibration Model in a Tandem Cold Rolling Mill

Xing Lu, Jie Sun, Guangtao Li, Zhenhua Wang, and Dianhua Zhang

The State Key Laboratory of Rolling and Automation, Northeastern University, Shenyang 110819, Liaoning, China

Correspondence should be addressed to Jie Sun; sunjie@ral.neu.edu.cn

Received 24 October 2018; Revised 21 January 2019; Accepted 24 January 2019; Published 17 February 2019

Academic Editor: Roger Serra

Mill chatter in tandem cold rolling mill is a major rejection to the quality and production of the strips. In most mill vibration models, either the roll mass is usually limited to vibrate in vertical direction and vertical-horizontal directions, or the multiple rolls system is simplified to a single mass system. However, the torsional chatter is also a typical type of mill chatter, and the presence of intermediate roll and backup roll will affect the overall vibration of the mill structure system. In this paper, a newly cold rolling mill vibration model coupled with the dynamic rolling processing model and nonlinear vibration model is proposed with the consideration of dynamic coupling and nonlinear characteristics of the rolling process, multiroll equilibrium, and roll movement in both vertical-horizontal-torsional directions. By using Hopf bifurcation theorem and Routh–Hurwitz determinant, the existence of the Hopf bifurcation point of the mill vibration system and bifurcation characteristics are analyzed. At last, the influence of different rolling conditions on the stability of the coupled mill system is investigated, and these results can also be used to design an optimum rolling schedule and determine the appearance of mill chatter under certain rolling conditions.

1. Introduction

With the optimization and upgrading in the steel industry, the urgent demands for high strip quality and strip yield have become more stringent. However, due to the abnormal mill vibration, the quality and production of the strip have been restricted. Abnormal vibration in the tandem cold rolling mill is a common and complicated phenomenon. Researchers tend to consider that mill chatter is a typical self-excited vibration [1–3], which consists of third-octave mode chatter (150–250 Hz), fifth-octave mode chatter (500–700 Hz), and torsional chatter.

In the mill chatter analysis, the most typical models are finite element method (FEM) models, multiple degrees of freedom structure model, and mill drive system torsional structure models. Niroomand et al. [4–6] studied the third-octave mode chatter and fifth-octave mode chatter in the vertical direction by using FEM analysis models. In these papers, the backup roll was set as a mass point, and a connector was used to represent the displacement of the backup roll and mill stand housing. In FEM models, the structure mode coupling characteristics cannot be fully reflected. For most vertical vibration models, the mill stand was modeled with multiple degrees of freedom. Kapil et al. [7] used the further simplified structure model to analyze the frequency response in detail. Kimura et al. [8, 9] and Heidari et al. [10–13] illustrated the influence of lubrication characteristic on mill chatter. However, in these studies, only the vertical vibration phenomena were investigated. But, in the actual rolling process, the roll vibrated in more than one direction. So, it is necessary to establish a coupled chatter model which allows roll to vibrate in two directions. Yun et al. presented a dynamic coupled chatter model that allows roll vibrate in two directions and investigated the relationship between mill vibration and the rolling conditions [2]. Kim et al. [14] proposed a vertical and horizontal coupling chatter model and analyzed the dynamic response of roll displacement under different rolling pressures. In the research of torsional vibration on the rotating shaft, Krot [15] analyzed the nonlinear torsional vibration caused by angular and radial wear in gear. Liu et al. [16, 17] established a multiple degree of freedom of mill main drive system and studied the torsional chatter characteristics in the main drive system of the mill stand.

Bifurcation was an important theory of nonlinear field, which implied the sudden change of the topological property

of the dynamic system when the parameters change in the dynamic characteristic system. Hopf bifurcation was a typical type of bifurcation system. It was named after the name of the German mathematician Eberhard Hopf who proposed the concept. It referred to the bifurcation of the periodic oscillation and the appearance of a stable limit cycle, which is caused by the dynamic change of the parameter [18]. Hopf bifurcation had theoretical value not only in the dynamic bifurcation research but also closely related to the generation of self-excited vibration in engineering. Lee found that the Hopf bifurcation phenomenon in the wing flutter system was the main cause of the casing vibration [19], and the magnitude of the pitch angle played an important role in this vibration problem. The characteristics and localization of multiple pendulum-type centrifugal pendulum vibration absorbers were investigated to suppress torsional vibrations of shaft by using Hopf bifurcation theory [20]. Zhang and Dai used nonlinear creep theory to study bifurcation phenomenon and stability of China Railways High-speed vehicle (CRH-3) [21].

Many researchers have found that the dynamic rolling mill system was often accompanied with the generation of limit cycle when unstable oscillation occurs during rolling. So, Hopf bifurcation theorem was also introduced into the mill stand vibration analysis. Gao et al. [22, 23] established a dynamic model of rolling mill system and analyzed the Hopf bifurcation and mill stability. Liu et al. [24] established a dynamic vibration considering the torsional vibration of gear and the horizontal vibration of the roll, and the stability of the mill drive system was analyzed. Peng et al. [25] proposed a swing chatter model coupling the vertical-horizontal-torsional vibration and studied the influence of meshing impact force on the roll system stability.

Researchers have shown the existence of negative damping effects in mill structure. But the relationship between dynamic rolling conditions and damping coefficient is not clearly illustrated. Besides, the Hopf bifurcation phenomenon in the rolling mill drive vibration system is an important cause of system instability. The occurrence of the Hopf bifurcation limit cycle determines the stability and stable range of the mill. Then, vibration problem caused by negative damping effect can be transformed into the analysis of the Hopf bifurcation phenomenon in the vibration model. Scholars have done plenty scientific works about vibration in cold rolling. However, most of those theses were either concentrated on vertical vibration or torsional vibration, or the whole roll system was simplified by one single roll. Therefore, a further multiroll and nonlinear vertical-horizontal-torsional coupled vibration model of the universal crown control mill (UCM mill) needs to be proposed and analyzed. And based on this proposed rolling mill vibration model, the bifurcation phenomenon and stability of the mill system is analyzed to illustrate the dynamic characteristics of the UCM mill more comprehensively.

2. Dynamic Rolling Process Model

The geometry of roll gap in the cold rolling is presented in Figure 1. O is the original center of the work roll, and O' is the new center of the flattened roll. x_{in}, x_n, and x_{out} are the entry position, neutral position, and exit position. α and γ are the bite angle and neutral angle. v_{in} and v_{out} are the strip speed at the entry and exit point. h_{in}, h_n, and h_{out} are the strip thickness at the entry, neutral, and exit point. x_w is the dynamic vibration displacement of work roll in the horizontal direction. y_w is the dynamic vibration displacement of work roll in the vertical direction. T_f and T_b are the front and back tension.

In cold rolling, Hitchcock indicated that the flattened work roll radius R' can be evaluated as

$$R' = R\left\{1 + \frac{16\left(1-\upsilon^2\right)}{\pi E_1}\frac{P}{w\cdot\left(h_{\text{in}}-h_{\text{out}}\right)}\right\}, \tag{1}$$

where υ is Poisson's ratio; in this research $\upsilon = 0.3$. w is the width of the strip. E_1 is Young's modulus of the work roll. P is the total rolling force. R and R' are the work roll original radius and roll flattened radius.

Considering work roll elastic deformation, the contact arc length in the roll gap is

$$l' = \sqrt{R\left(h_{\text{in}}-h_{\text{out}}\right)+\left(8\frac{1-\upsilon^2}{\pi E_1}R\overline{p}\right)^2} + 8\frac{1-\upsilon^2}{\pi E_1}R\overline{p}, \tag{2}$$

where $\overline{p}$ is the average rolling force.

Assuming the contour of the roll gap can be written as a parabolic curve, the strip thickness at any point in the roll gap can be determined as [11]

$$h(x) = h_{\text{c}} + \frac{x^2}{R'}, \tag{3}$$

where h_{c} is the roll gap spacing distance along the centerline of the work roll and x is the position of the strip along the rolling direction in the roll gap.

From equation (3), the entry position of the strip can be given as

$$x_{\text{in}} = x_w - \sqrt{R'\left(h_{\text{in}}-h_{\text{c}}\right)}. \tag{4}$$

So, the dynamic roll gap spacing of the roll centerline can be related as [11, 22]

$$h_{\text{out}} = h_{\text{c}} + 2y_w. \tag{5}$$

Based on equation (5) and considering mill elastic deformation, the variation of strip thickness at exit is expressed as

$$dh_{\text{out}} = 2y_w + \frac{dP}{K_w}, \tag{6}$$

where dP is the rolling force variation and k_w is the equivalent spring constant of the work roll.

And strip thickness at the neutral point can be calculated by [8]

$$h_n = \frac{h_{\text{in}}+h_{\text{out}}}{2} - \frac{1}{2\mu}\log\left(\frac{h_{\text{in}}}{h_{\text{out}}}\times\frac{1-\left(T_f/k_{h_{\text{out}}}\right)}{1-\left(T_b/k_{h_{\text{in}}}\right)}\right). \tag{7}$$

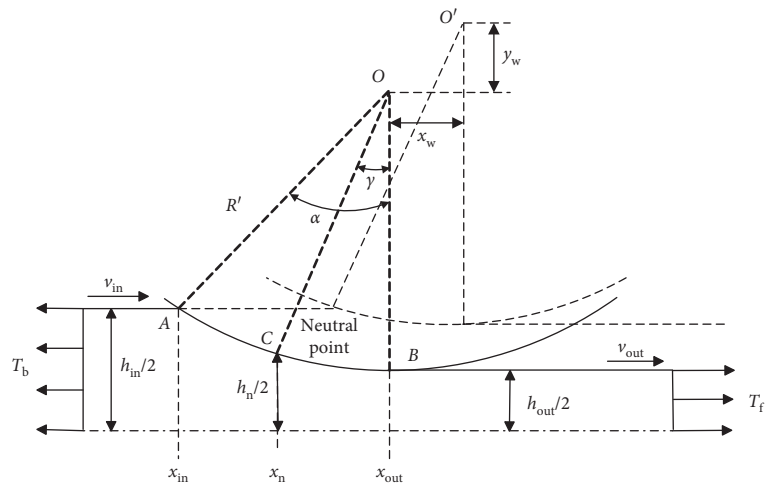

Figure 1: Vibration geometry model of the roll gap.

The neutral angle is calculated by

$$\gamma = \sqrt{\frac{h_{out}}{R'}} \times \tan\left(\sqrt{\frac{h_{out}}{R'}} \times \frac{h_n}{2}\right), \tag{8}$$

where $k_{h_{in}}$ and $k_{h_{out}}$ are the deformation resistance at strip entry and exit position and μ is the friction coefficient in the roll gap.

Based on equation (7), strip thickness fluctuation at the neutral point can be expressed as

$$\begin{aligned} dh_n &= \frac{\partial h_n}{\partial h_{in}} dh_{in} + \frac{\partial h_n}{\partial h_{out}} dh_{out} + \frac{\partial h_n}{\partial T_f} dT_f + \frac{\partial h_n}{\partial T_b} dT_b \\ &= \left(\frac{1}{2} - \frac{1}{2\mu h_{in}}\right) dh_{in} + \left(\frac{1}{2} + \frac{1}{2\mu h_{out}}\right) dh_{out} \\ &\quad + \frac{1}{2\mu\left(k_{h_{out}} - T_f\right)} dT_f - \frac{1}{2\mu\left(k_{h_{in}} - T_b\right)} dT_b. \end{aligned} \tag{9}$$

Considering the mass conservation law to the mass flow continuity equation,

$$V_r h_n = v_{in} h_{in} = v_{out} h_{out}, \tag{10}$$

where V_r is the work roll circumference velocity.

The strip speed variation at the entry and exit can be expressed as [8]

$$\begin{cases} dv_{in} = \dfrac{V_r}{h_{in}} dh_n, \\ \\ dv_{out} = \dfrac{V_r}{h_{out}^2} \left(h_{out} dh_n - h_n dh_{out}\right). \end{cases} \tag{11}$$

According to Hooke's law, the variation of tension is proportional to integral of speed difference between entry of i stand and exit of $i-1$ stand [26]. Assuming the exit speed of $i-1$ stand and entry speed of $i+1$ stand are always kept constant, the tension variation at the entry and exit can be expressed as

$$\begin{cases} dT_{f,i} = -\dfrac{E_2}{5.5025} \int dv_{out,i} dt, \\ \\ dT_{b,i} = \dfrac{E_2}{5.5025} \int dv_{in,i} dt, \end{cases} \tag{12}$$

where subscript i means i stand. And in this research, the strip length between i and $i+1$ stand is 5.5025 m.

In the most rolling mill vibration models, the friction coefficient was usually set as a constant value. However, in the cold rolling, the lubrication characteristics in the roll gap were significantly different under the high rolling speed and low speed. Sims and Arthur [27] found that when the rolling speed was higher than 0.25 m/s, the friction coefficient showed a nonlinear characteristic which is caused by unsteady rolling conditions. As a result, it is necessary to investigate the dynamic vibration stability in the UCM mill with the consideration of nonlinear friction characteristics. Considering the roll wear and other conditions into consideration, the friction coefficient in this research is obtained by [28]

$$\begin{aligned} \mu &= \left(\mu_0 + \mu_V \cdot e^{-(V_r/V_0)}\right) \cdot \left[1 + c_R \cdot \left(R_a - R_{a_0}\right)\right] \\ &\quad \cdot \left(1 + \frac{c_W}{1 + (L/L_0)}\right), \end{aligned} \tag{13}$$

where μ_0 and μ_V are the basic friction coefficient that related to lubrication and lubrication coefficient related to rolling speed, V_0 is the basic rolling speed, R_a and R_{a_0} are actual work roll roughness and roughness of unused work roll, C_R is the work roll roughness coefficient, c_W is the coefficient related to cumulative rolling strip length, and L and L_0 are the cumulative rolling strip length of work roll and datum rolling length.

The rolling force is calculated by Bland-Ford-Hill equation [29, 30]:

$$P = wl' \overline{k} Q_p n_t, \tag{14}$$

where

$$\begin{cases} Q_p = 1.08 + 1.79\varepsilon\mu\sqrt{\dfrac{R'}{h_{\text{in}}}} - 1.02\varepsilon, \\ n_t = 1 - \dfrac{\left[(1-\mu_t)T_f + \mu_t T_b\right]}{\overline{k}}, \quad \mu_t = 0.7, \\ \varepsilon = \dfrac{h_{\text{in}} - h_{\text{out}}}{h_{\text{in}}}, \end{cases} \tag{15}$$

and $\overline{k}$ is the deformation resistance of the rolling strip. In this research, deformation resistance of the strip is expressed by the following equation:

$$\overline{k} = \left(A + B \cdot \varepsilon_\Sigma\right)\left(1 - C \cdot e^{-D\cdot\varepsilon_\Sigma}\right), \tag{16}$$

where ε_Σ is average strain, which can be given by $\varepsilon_\Sigma = (2/\sqrt{3}) \cdot \ln(H_0/\overline{h})$, $\overline{h} = (h_{\text{in}} + 2h_{\text{out}}/3)$. A, B, C, and D are references in deformation resistance model. In this research, $A = 500.00$ MPa, $B = 179.00$ MPa, $C = 0.20$, and $D = 5.00$. H_0 is the thickness of the raw material.

The investigation of UCM mill showed that No. 4 and No. 5 stand chatter frequently, so a comprehensive mill vibration monitoring test was implemented in a 1450 mm UCM plant by using CTC-type accelerometer sensors. The accelerometer sensors were mounted on the work roll bearings of No. 5 stand. When rolling the most common products of 0.35 mm strip in this plant, the vibration signals during the stable rolling stage are shown in Figure 2. It illustrated that although the horizontal rolling force was relatively small compared with the vertical rolling force, the horizontal rolling force was still big enough. Therefore, it was sufficiently significant to establish a comprehensive model which allows the rolls to vibrate in both horizontal and vertical directions.

Considering the dynamic equilibrium of strip in x direction, the horizontal rolling force can be calculated as follows:

$$\begin{aligned} P_x &= \int_0^a P\sin\theta d\theta + \int_\gamma^a P\mu\cos\theta d\theta - \int_0^\gamma P\mu\cos\theta d\theta \\ &= \frac{w}{2}\left(T_f h_{\text{out}} - T_b h_{\text{in}}\right). \end{aligned} \tag{17}$$

The vertical rolling force can be written as

$$\begin{aligned} P_y &= \int_0^\alpha P\cos\theta \mathrm{d}\theta + \int_\gamma^\alpha P\mu\sin\theta \mathrm{d}\theta - \int_0^\gamma P\mu\sin\theta \mathrm{d}\theta \\ &= wl'\overline{k}Q_p n_t\left(\int_0^\alpha \cos\theta \mathrm{d}\theta + \int_\gamma^\alpha \mu\sin\theta \mathrm{d}\theta - \int_0^\gamma \mu\sin\theta \mathrm{d}\theta\right) \\ &= wl'\overline{k}Q_p n_t\left(\int_0^\alpha \cos\theta \mathrm{d}\theta - \mu\cos\alpha + 2\mu\cos\gamma - \mu\right). \end{aligned} \tag{18}$$

Considering that the bite angle α and neutral angle γ are extremely small, it assumed that the vertical rolling force is equal to the total rolling force [14, 22], so equation (18) can be expressed as

$$P_y \approx wl'\overline{k}Q_p n_t \int_0^\alpha \cos\theta \mathrm{d}\theta \approx wl'\overline{k}Q_p n_t = P. \tag{19}$$

Assuming the thickness fluctuation and tension variation are caused by roll gap vibration as separated disturbances, the deviation of the rolling force in the x direction can be written as

$$dP_x = \frac{\partial P_x}{\partial h_{\text{in}}}dh_{\text{in}} + \frac{\partial P_x}{\partial h_{\text{out}}}dh_{\text{out}} + \frac{\partial P_x}{\partial T_b}\mathrm{d}T_b + \frac{\partial P_x}{\partial T_f}\mathrm{d}T_f. \tag{20}$$

Based on equation (17), the deviation of the rolling force in the x direction can be also expressed as

$$dP_x = -\frac{wT_b}{2}dh_{\text{in}} + wT_f dy_w - \frac{wh_{\text{in}}}{2}dT_b + \frac{wh_{\text{out}}}{2}dT_f. \tag{21}$$

The variation of the rolling force in the y direction can be defined as

$$dP_y = \frac{\partial P}{\partial h_{\text{in}}}dh_{\text{in}} + \frac{\partial P}{\partial h_{\text{out}}}dh_{\text{out}} + \frac{\partial P}{\partial T_f}dT_f + \frac{\partial P}{\partial T_b}dT_b, \tag{22}$$

where

$$\begin{cases} \dfrac{\partial P}{\partial h_{\text{in}}} = wl'\overline{k}n_t\left(-\dfrac{1.79}{2}\mu\sqrt{\dfrac{R'}{h_{\text{in}}^3}} + \dfrac{3}{2}\times 1.79\mu h_{\text{out}}\sqrt{\dfrac{R'}{h_{\text{in}}^5}} - 1.02\dfrac{h_{\text{out}}}{h_{\text{in}}^2}\right), \\ \dfrac{\partial P}{\partial h_{\text{out}}} = wl'\overline{k}n_t\left(-1.79\dfrac{\mu}{h_{\text{in}}}\sqrt{\dfrac{R'}{h_{\text{in}}}} + 1.02\dfrac{1}{h_{\text{in}}}\right), \\ \dfrac{\partial P}{\partial T_b} = -0.7wl'Q_p, \\ \dfrac{\partial P}{\partial T_f} = -0.3wl'Q_p. \end{cases} \tag{23}$$

The rolling torque of the upper roll system can be deduced as [23, 25]

$$\begin{aligned} M &= w\int_0^\gamma \mu\overline{p}R\ d\theta - w\int_\gamma^\alpha \mu\overline{p}R\ d\theta \\ &= w\mu\overline{p}R(2\gamma - \alpha) \\ &= P\mu R(2\gamma - \alpha). \end{aligned} \tag{24}$$

Considering the bite angle α and neutral angle γ are extremely small, $\alpha \approx \sqrt{(h_{\text{in}} - h_{\text{out}}/R')}$, $\gamma \approx \sin\gamma = (x_w - x_n/R')$, and $x_n = \sqrt{R'(h_n - h_c)}$.

Also, the variation of the rolling torque can be calculated by

$$dM = \frac{\partial M}{\partial h_{\text{in}}}dh_{\text{in}} + \frac{\partial M}{\partial h_{\text{out}}}dh_{\text{out}} + \frac{\partial M}{\partial T_f}dT_f + \frac{\partial M}{\partial T_b}dT_b + \frac{\partial M}{\partial x_w}dx_w, \tag{25}$$

where

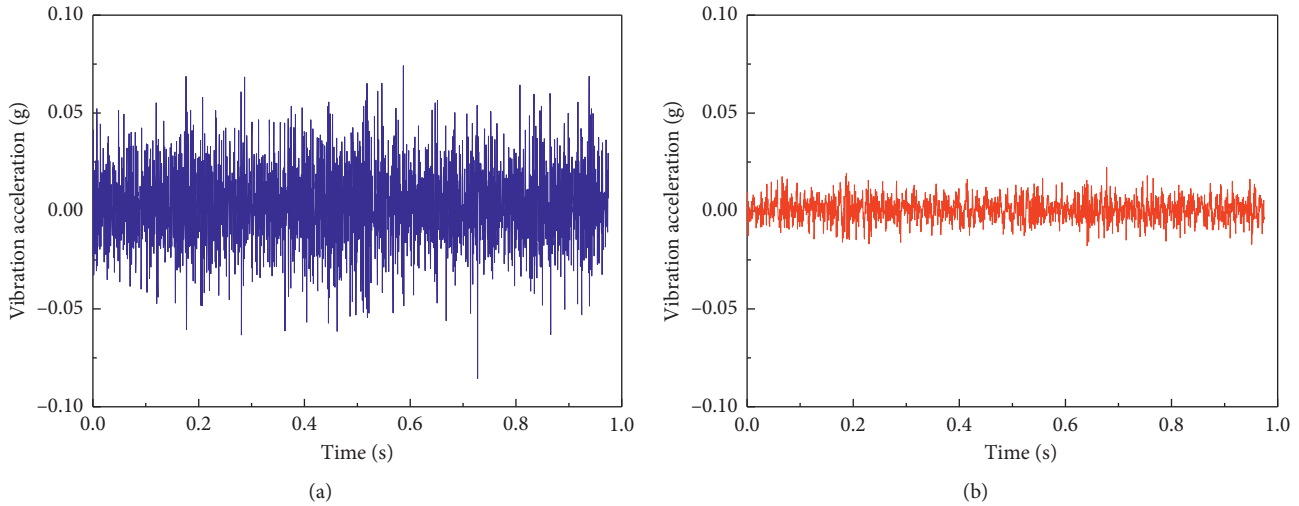

Figure 2: Time domain vibration signal of the work roll: (a) vibration acceleration in the vertical direction; (b) vibration acceleration in the horizontal direction.

$$\begin{cases} \dfrac{\partial M}{\partial h_{\text{in}}} = wl'\bar{k}n_t(2\gamma-\alpha)\left(-\dfrac{1.79}{2}\mu\sqrt{\dfrac{R'}{h_{\text{in}}^3}}+\dfrac{3}{2}\times 1.79\mu h_{\text{out}}\sqrt{\dfrac{R'}{h_{\text{in}}^5}}\right. \\ \qquad \left. -1.02\dfrac{h_{\text{out}}}{h_{\text{in}}^2}\right)-\dfrac{1}{2}wl'\bar{k}Q_p n_t\mu R\dfrac{1}{\sqrt{(h_{\text{in}}-h_{\text{out}})R'}}, \\ \dfrac{\partial M}{\partial h_{\text{out}}} = wl'\bar{k}n_t(2\gamma-\alpha)\left(-1.79\dfrac{\mu}{h_{\text{in}}}\sqrt{\dfrac{R'}{h_{\text{in}}}}+1.02\dfrac{1}{h_{\text{in}}}\right) \\ \qquad +\dfrac{1}{2}wl'\bar{k}Q_p n_t\mu R\dfrac{1}{\sqrt{(h_{\text{in}}-h_{\text{out}})R'}}, \\ \dfrac{\partial M}{\partial T_b} = -0.7wl'Q_p\mu R(2\gamma-\alpha), \\ \dfrac{\partial M}{\partial T_f} = -0.3wl'Q_p\mu R(2\gamma-\alpha), \\ \dfrac{\partial M}{\partial x_w} = wl'\bar{k}Q_p n_t\mu R\left(2\dfrac{1}{R'}-\alpha\right). \end{cases} \tag{26}$$

The calculated rolling conditions in this research are shown in Table 1. The grade of rolling strip is MRT5, and the exit strip width is 900 mm.

Figure 3 shows the comparison of calculated rolling force in this rolling process model and actual rolling force in the experiment. The rolling conditions are shown in Table 1. As shown in Figure 3, the maximum relative error between actual rolling force and calculated rolling force is 7.23%. The comparative results of the simulation and experimental data show that this chatter model has a high accuracy.

3. Dynamic Nonlinear Vibration Model of the UCM Mill

In most vibration research studies, the rolling mill stand was simplified as a mass-spring system. To investigate the displacements of each roll and interaction between rolls, a model with multiple degrees of freedom is necessary. However, with the consideration of the symmetry of the mill structure along the rolling pass line, the multiple degrees of freedom chatter model can be simplified. Figure 4 is the simplified nonlinear vertical-horizontal-torsional coupled vibration model considering the roll movement in more than one direction.

As shown in Figure 4, the top work roll (WR) would vibrate in both vertical and horizontal directions. While the intermediate roll (IMR) and backup roll (BUR) were not allowed to vibrate in horizontal direction due to the assembly and restriction of the roll bearings [25].

A horizontal roll vibration displacement of WR is generated due to the installation offset of e between WR and IMR, and the equivalent spring constant in horizontal direction can be calculated by

Table 1: Rolling conditions.

Parameters	#1 stand	#2 stand	#3 stand	#4 stand	#5 stand
Entry thickness, h_{in} (mm)	2.000	1.269	0.762	0.460	0.300
Exit thickness, h_{out} (mm)	1.269	0.762	0.460	0.300	0.200
Rolling force, P (kN)	7838.863	8455.166	7781.567	7500.996	7722.711
Exit tension, T_f (MPa)	140.554	165.252	188.160	205.575	68.000
Entry tension, T_b (MPa)	55.000	140.554	165.252	188.160	205.575
Friction coefficient, μ	0.065	0.060	0.040	0.030	0.020
Roll velocity, V_r (m s^{-1})	3.381	5.652	9.425	14.441	22.121
Strip entry speed, v_{in} (m s^{-1})	2.250	3.546	5.903	9.774	14.977

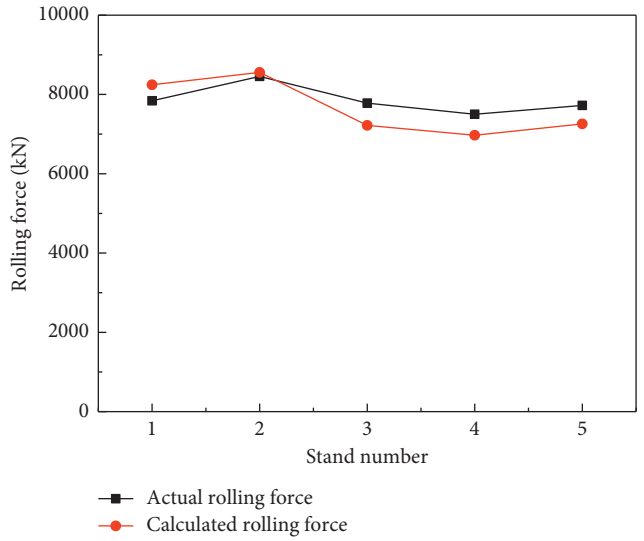

Figure 3: Comparison between the actual rolling force and calculated rolling force.

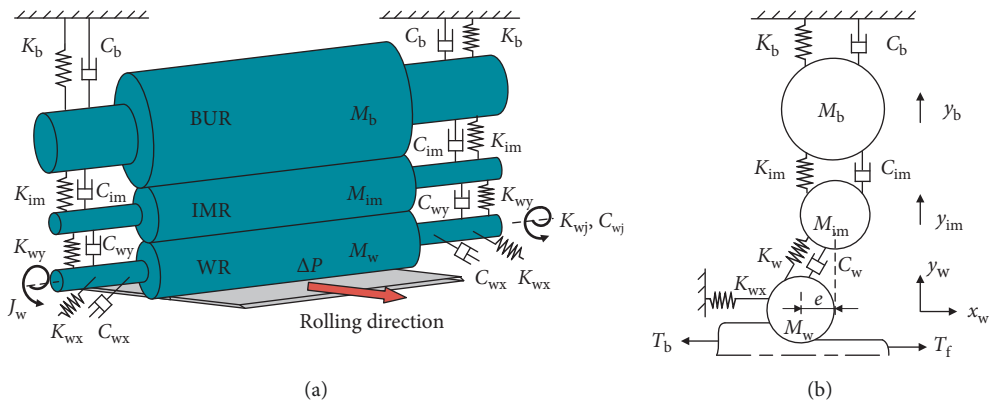

Figure 4: Geometry of the vertical-horizontal-torsional vibration model: (a) simplified vertical-horizontal-torsional coupled vibration model; (b) geometry of coupled vibration model in x-y direction.

$$K_{wx} = \frac{e}{R_w + R_{\text{im}}} K_w, \tag{27}$$

where R_w and R_{im} are the roll radius of work roll and intermediate roll and K_w is the contact spring constant between upper work roll and intermediate roll.

With the consideration of the coupling movement of the rolls in both vertical, horizontal, and torsional directions, the dynamic equilibrium equation of the upper roll system was given by

$$\begin{cases} M_w \ddot{x}_w + C_{wx}\dot{x}_w + K_{wx}x_w = \Delta P_x, \\ M_w \ddot{y}_w + C_{wy}(\dot{y}_w - \dot{y}_{\text{im}}) + K_{wy}(y_w - y_{\text{im}}) = \Delta P_y, \\ M_{\text{im}} \ddot{y}_{\text{im}} - C_{wy}(\dot{y}_w - \dot{y}_{\text{im}}) + C_{\text{im}}(\dot{y}_{\text{im}} - \dot{y}_b) \\ \quad - K_{wy}(y_w - y_{\text{im}}) + K_{\text{im}}(y_{\text{im}} - y_b) = 0, \\ M_b \ddot{y}_b - C_{\text{im}}(\dot{y}_{\text{im}} - \dot{y}_b) + C_b \dot{y}_b - K_{\text{im}}(y_{\text{im}} - y_b) \\ \quad + K_b y_b = 0, \\ J_w \ddot{\theta}_w + C_{wj}\dot{\theta}_w + K_{wj}\theta_w = \Delta M, \end{cases} \tag{28}$$

where x_w is the WR vibration displacement in horizontal direction, y_w, y_{im}, and y_b are the vibration displacement of WR, IMR, and BUR in vertical direction, θ_w is the WR torsional vibration angular displacement, ΔP_x and ΔP_y are the fluctuation of rolling force in horizontal and vertical directions, ΔM is the variation of rolling torque, and M_w, M_{im}, and M_b are the mass of work roll, intermediate roll, and backup roll, respectively.

The mill stand spring constant is the total stiffness of the whole rolling mill consisting of all the rolls. The mill spring constant (K) is measured by a stiffness calibration test. The spring constants of work roll (K_w), intermediate roll (K_{im}), and backup roll (K_b) are calculated by an FEM model of the UCM mill [5, 6, 12]. The roll vibration displacement under different rolling forces was obtained by a simulation experiment. The spring constants of the work roll, intermediate roll, and backup roll were obtained by analyzing the dynamic roll vibration displacement under different rolling forces.

Damping coefficients of the intermediate and backup rolls are calibrated by a simulation program [31, 32]. First,

the dynamic differential equation of the system is regularized to obtain the equivalent damping matrix. Then, the damping regular matrix is transformed into the original coordinate system, and let the damping ratio be 0.03. Finally, the equivalent damping value of the roll system is calculated. Work roll rotational inertia mass, work roll rotational spring constant, and work roll rotational damping coefficient are obtained from the work of Zeng et al. [23], as the design and mill structure of rolling stands are similar to one another. The roll diameters and work roll installation offset are obtained from the UCM rolling mill installation drawings. Table 2 shows the structure specifications of the UCM mill in equation (28).

Equation (28) is the nonlinear dynamic equation of the vertical-horizontal-torsional coupled vibration model. Convert the above differential equation into the following state matrix form:

$$\dot{X} = F(X, \mu) + Hdh_{\text{in}}, \tag{29}$$

where

$$X = \left[x_w, \dot{x}_w, y_w, \dot{y}_w, y_{\text{im}}, \dot{y}_{\text{im}}, y_b, \dot{y}_b, \theta_w, \dot{\theta}_w, dT_f, dT_b\right]^{\text{T}} = \left[x_1, x_2, x_3, \ldots, x_{12}\right]^{\text{T}},$$

$$H = \left[0, -\frac{wT_b}{2M_w}, 0, \frac{\partial P}{\partial h_{\text{in}} M_w}, 0, 0, 0, 0, 0, \frac{\partial M}{\partial h_{\text{in}} J_w}, 0, 0\right]^{\text{T}},$$

$$F = \begin{bmatrix} 0 & 1 & 0 & 0 & 0 & 0 & 0 & 0 & 0 & 0 & 0 & 0 \\ F_{2,1} & F_{2,2} & F_{2,3} & 0 & 0 & 0 & 0 & 0 & 0 & 0 & 0 & 0 \\ 0 & 0 & 0 & 1 & 0 & 0 & 0 & 0 & 0 & 0 & 0 & 0 \\ 0 & 0 & F_{4,3} & F_{4,4} & F_{4,5} & F_{4,6} & 0 & 0 & 0 & 0 & 0 & 0 \\ 0 & 0 & 0 & 0 & 0 & 1 & 0 & 0 & 0 & 0 & 0 & 0 \\ 0 & 0 & F_{6,3} & F_{6,4} & F_{6,5} & F_{6,6} & F_{6,7} & F_{6,8} & 0 & 0 & 0 & 0 \\ 0 & 0 & 0 & 0 & 0 & 0 & 0 & 1 & 0 & 0 & 0 & 0 \\ 0 & 0 & 0 & 0 & F_{8,5} & F_{8,6} & F_{8,7} & F_{8,8} & 0 & 0 & 0 & 0 \\ 0 & 0 & 0 & 0 & 0 & 0 & 0 & 0 & 0 & 1 & 0 & 0 \\ 0 & F_{10,2} & F_{10,3} & 0 & 0 & 0 & 0 & 0 & F_{10,9} & F_{10,10} & F_{10,11} & F_{10,12} \\ 0 & 0 & F_{11,3} & 0 & 0 & 0 & 0 & 0 & 0 & 0 & F_{11,11} & F_{11,12} \\ 0 & 0 & F_{12,3} & 0 & 0 & 0 & 0 & 0 & 0 & 0 & F_{12,11} & F_{12,12} \end{bmatrix},$$

$$F_{2,1} = -\frac{K_{wx}}{M_w},$$

$$F_{2,2} = -\frac{C_{wx}}{M_w},$$

$$F_{2,3} = \frac{wT_f}{M_w},$$

$$F_{4,3} = \frac{2(\partial P/\partial h_{\text{out}}) - K_{wy}}{M_w},$$

$$F_{4,4} = \frac{-C_{wy}}{M_w},$$

$$F_{4,5} = \frac{K_{wy}}{M_w},$$

$$F_{4,6} = \frac{C_{wy}}{M_w},$$

$$F_{6,3} = \frac{K_{wy}}{M_{\text{im}}},$$

$$F_{6,4} = \frac{C_{wy}}{M_{im}},$$

$$F_{6,5} = -\frac{K_{wy} + K_{\text{im}}}{M_{\text{im}}},$$

$$F_{6,6} = -\frac{C_{wy} + C_{\text{im}}}{M_{\text{im}}},$$

$$F_{6,7} = \frac{K_{\text{im}}}{M_{\text{im}}},$$

$$F_{6,8} = \frac{C_{\text{im}}}{M_{\text{im}}},$$

$$F_{8,5} = \frac{K_{\text{im}}}{M_b},$$

$$F_{8,6} = \frac{C_{\text{im}}}{M_b},$$

$$F_{8,7} = -\frac{K_{\text{im}} + K_b}{M_b},$$

$$F_{8,8} = -\frac{C_{\text{im}} + C_b}{M_b},$$

$$F_{10,2} = \frac{\partial M}{J_w \partial x_w},$$

$$F_{10,3} = \frac{2\partial M}{J_w \partial h_{\text{out}}},$$

$$F_{10,9} = -\frac{K_{wj}}{J_w},$$

$$F_{10,10} = -\frac{C_{wj}}{J_w},$$

$$F_{10,11} = \frac{\partial M}{J_w \partial T_f},$$

$$F_{10,12} = \frac{\partial M}{J_w \partial T_b},$$

$$F_{11,3} = -\frac{2E_2 V_r\left((\partial h_n/\partial h_{\text{out}})h_{\text{out}} - h_n\right)}{5.5025 h_{\text{out}}^2},$$

$$F_{11,11} = -\frac{E_2 V_r\left(\partial h_n/\partial T_f\right)}{5.5025 h_{\text{out}}},$$

$$F_{11,12} = -\frac{E_2 V_r\left(\partial h_n/\partial T_b\right)}{5.5025 h_{\text{out}}},$$

$$F_{12,3} = \frac{2E_2 V_r\left(\partial h_n/\partial h_{\text{out}}\right)}{5.5025 h_{\text{in}}},$$

$$F_{12,11} = \frac{E_2 V_r\left(\partial h_n/\partial T_f\right)}{5.5025 h_{\text{in}}},$$

$$F_{12,12} = \frac{E_2 V_r\left(\partial h_n/\partial T_f\right)}{5.5025 h_{\text{in}}}. \tag{30}$$

Then, equation (29) is the nonlinear dynamic state equation of the vertical-horizontal-torsional coupled vibration system considering the nonlinear characteristic during the rolling process, the movement of rolls in both vertical-horizontal directions, and the torsional vibration.

4. Analysis of Vibration Stability of the Roll System

4.1. Hopf Bifurcation Parameter Calculation. The friction characteristic would cause the instability of the dynamic state equation, so in this research μ has been chosen as the

Table 2: Structure specifications of the UCM mill.

Parameters	Value
Work roll mass, M_w (Kg)	3914
Intermediate roll mass, M_{im} (Kg)	5410
Backup roll mass, M_b (Kg)	31330
Work roll contact spring constant, K_w (N m^{-1})	0.91×10^{10}
Intermediate roll spring constant, K_{im} (N m^{-1})	1.03×10^{10}
Backup roll spring constant, K_b (N m^{-1})	5.85×10^{10}
Work roll damping coefficient x direction, C_{wx} (N·s m^{-1})	5.00×10^{4}
Work roll damping coefficient in y direction, C_{wy} (N·s m^{-1})	1.64×10^{5}
Intermediate roll damping coefficient, C_{im} (N·s m^{-1})	5.70×10^{5}
Backup roll damping coefficient, C_b (N·s m^{-1})	5.10×10^{6}
Work roll rotational inertia mass, Jw (Kg·m^2)	1381
Work roll rotational spring constant, K_{wj} (N·m·rad^{-1})	7.90×10^{6}
Work roll rotational damping coefficient, C_{wj} (N·m·s rad^{-1})	4178
Work roll diameter, R_w (mm)	212.5
Intermediate roll diameter, R_{im} (mm)	245
Backup roll diameter, R_b (mm)	650
Work roll installation offset, e (mm)	5

Hopf bifurcation parameter. Assuming the entry thickness of each stand is constant, the equilibrium point is $\overline{X}$, where $F(\overline{X}) = 0$. The system equilibrium point can be transformed to the origin by coordinate transformation, $X_0 = [0,0,0,0,0,0,0,0,0,0,0,0]^{\text{T}}$. Let $JF(X)$ be the Jacobian matrix of $F(X)$. So, the Hopf bifurcation can be obtained by judging all the eigenvalues of $JF(X)$. However, it is difficult to calculate the eigenvalues of $JF(X)$ since the calculation amount is quite large. Then, the Routh–Hurwitz determinant is used to calculate the Hopf bifurcation point [33].

The characteristic equation of Jacobian matrix $JF(X)$ of the dynamic vertical-horizontal-torsional coupling vibration model is assumed to be

$$a_{12}\lambda^{12} + a_{11}\lambda^{11} + \cdots + a_2\lambda^2 + a_1\lambda + a_0 = 0. \tag{31}$$

The main determinant

$$D_1 = a_1, D_2 = \begin{vmatrix} a_1 & a_0 \\ a_3 & a_2 \end{vmatrix}, \cdots D_i = \begin{vmatrix} a_1 & a_0 & \cdots & 0 \\ a_3 & a_2 & \cdots & 0 \\ \cdots & \cdots & \cdots & \cdots \\ a_{2i-1} & a_{2i-2} & \cdots & a_i \end{vmatrix}, \tag{32}$$

where $a_i = 0$ if $i < 0$ or $i > n$, and $a_{12} = 1$.

Assuming μ^* is the Hopf bifurcation, the Hopf bifurcation conditions are [23, 24, 34]

$$\begin{cases} a_0(\mu^*) > 0, D_1(\mu^*) > 0, \cdots, D_{n-2}(\mu^*) > 0, D_{n-1}(\mu^*) = 0, \\ \dfrac{d\Delta_{i-1}(\mu^*)}{d\mu} \neq 0. \end{cases} \tag{33}$$

According to these assumptions, the Hopf bifurcation point of μ^* occurs at $\mu^* = 0.0048$ and $\mu^* = 0.0401$.

4.2. Analysis of Stable Range of Friction. When the value of μ^* is smaller than the first bifurcation point of $\mu^* = 0.0048$, such as $\mu^* = 0.0040$, the response of work roll displacement and Hopf bifurcation diagram are shown in Figure 5. The roll displacement will diverge rapidly, and the equilibrium point of the equilibrium equation is unstable. Besides, as shown in Figure 5(b), the phase trajectory will disperse outward of the origin in a ring shape and the radius curvature of the phase trajectory increases gradually. It is concluded that the roll vibration system is unstable and mill chatter appears.

As shown in Figure 6(a), when $\mu^* = 0.0048$, the work roll displacement exhibits as an equal amplitude vibration, and the roll vibrates at its balanced position. This steady region refers to the maximum and minimum fluctuation range of work roll. Meanwhile, Figure 6(b) shows that the phase diagram will begin to converge toward a stable limit cycle. The strip will produce a slight thickness fluctuation within the quality requirements, and the mill system is stable under these rolling conditions.

When $\mu^* = 0.0300$, the roll system's time history response and the phase diagram are shown in Figure 7. It can be seen from these figures that the phase trajectory will converges toward a smaller and smaller circle near the origin point. The equilibrium point of work roll is asymptotically stable.

The roll system stability about the critical parameter of $\mu^* = 0.0401$ is shown in Figure 8. When at the critical Hopf bifurcation parameter, displacement of work roll firstly becomes larger and finally converges to an equal amplitude oscillation. The equilibrium point is unstable, and the Hopf bifurcation diagram presents a ring shape. However, dynamic range of the fixed limit cycle in Figure 8 is a little larger compared with Figure 6. This is mainly because the friction is bigger, and as a result, the fluctuation of the response rolling force ΔP_i under the friction coefficient of 0.0401 is much bigger.

The numerical solution of work roll displacement under the Hopf bifurcation point of $\mu^* = 0.0420$ is shown in Figure 9. The roll displacement will disperse outward all the time. Besides, the phase diagram of the work roll will disperse outward of the cycle, and the radius curvature of the phase trajectory increases gradually. It illustrates that the mill vibration system is unstable and mill chatter is produced.

When $\mu^* < 0.0048$, the roll system is unstable, and when $\mu^* = 0.0048$, the system is stable. So the Hopf bifurcation of $\mu^* = 0.0048$ is the subcritical bifurcation point, and $\mu^* = 0.0401$ is the supercritical bifurcation point.

Many researchers attribute the change of stability in rolling mill system to the sudden change of the rolling force fluctuation in dynamic equilibrium equation [11, 25, 35]. The optimal setting range of friction coefficient is 0.0048–0.0401, and mill chatter appears when the friction is either too high or too low. This is mainly due to the fluctuation of rolling force. When the friction is high, with the increase of friction coefficient, the neutral angle becomes bigger, and then the neutral point shifts to the entry side, so the distance between the entry and neutral point becomes shorter, and the variation of the entry speed decreases [11]. However, the exit forward slip and exit speed fluctuation will increase.

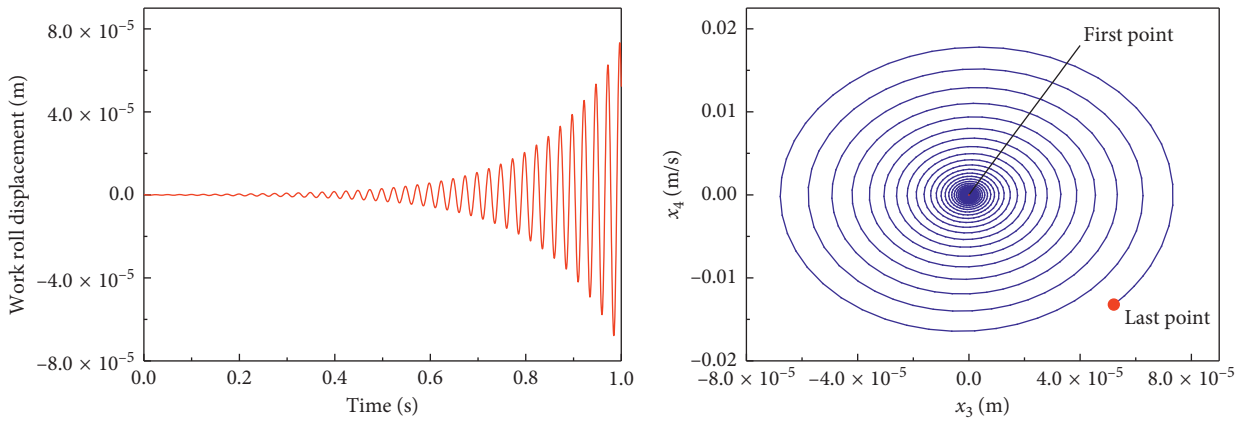

FIGURE 5: Dynamic response of the work roll displacement and the phase diagram under $\mu^* = 0.0040$: (a) time history of work roll displacement; (b) phase diagram.

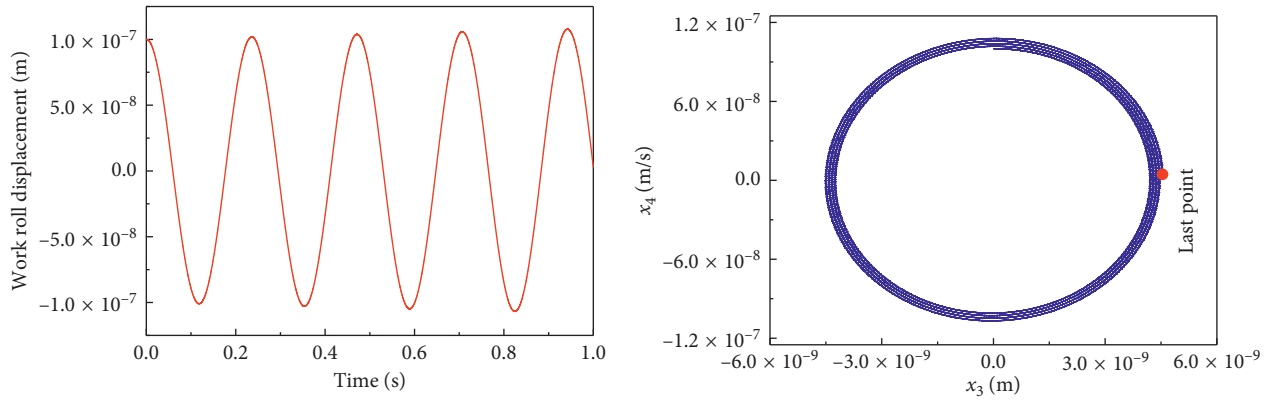

FIGURE 6: Dynamic response of the work roll displacement and the phase diagram under $\mu^* = 0.0048$: (a) time history of work roll displacement; (b) phase diagram.

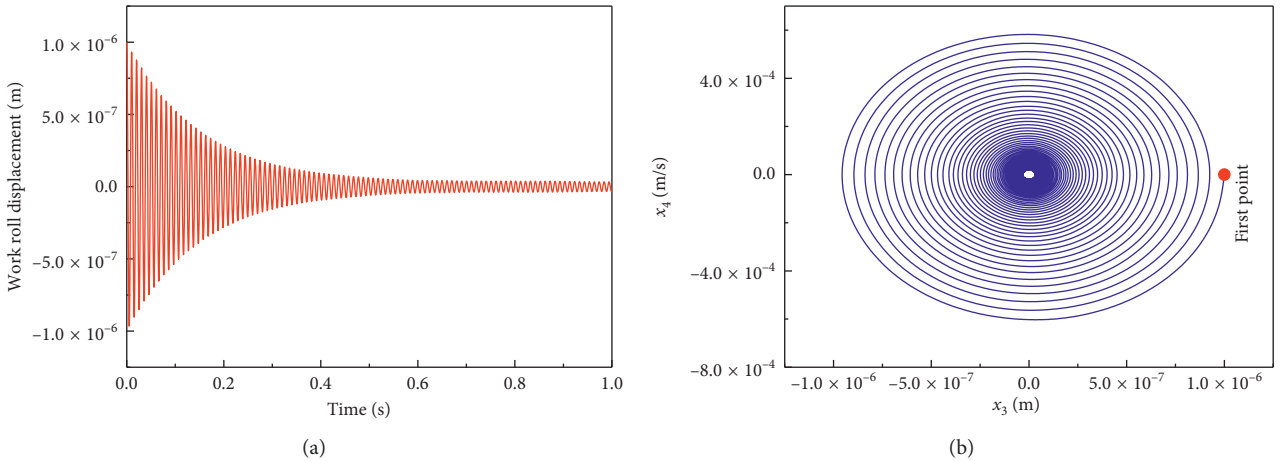

FIGURE 7: Dynamic response of the work roll displacement and the phase diagram under $\mu^* = 0.0300$: (a) time history of work roll displacement; (b) phase diagram.

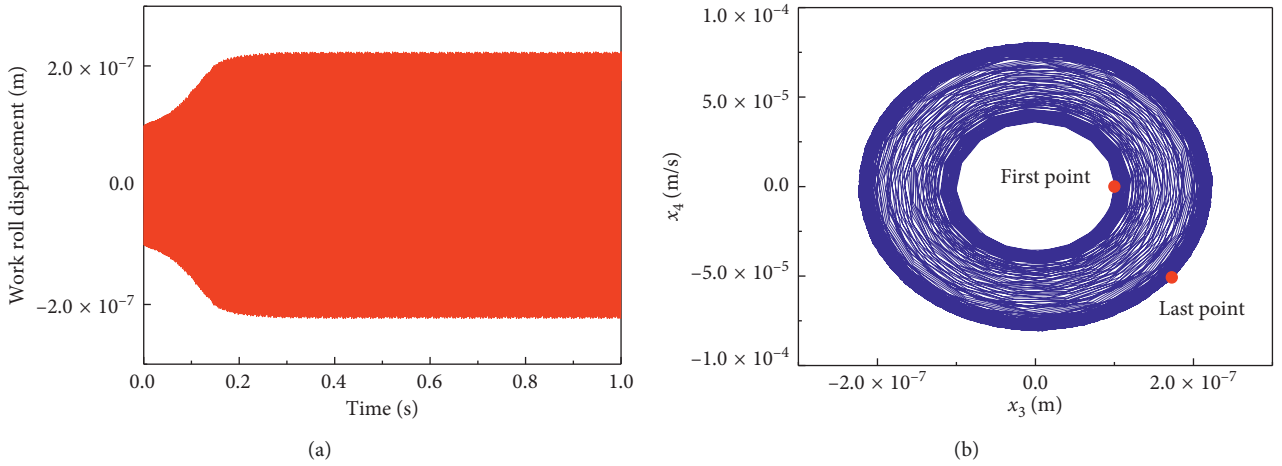

Figure 8: Dynamic response of the work roll displacement and the phase diagram under $\mu^* = 0.0401$: (a) time history of work roll displacement; (b) phase diagram.

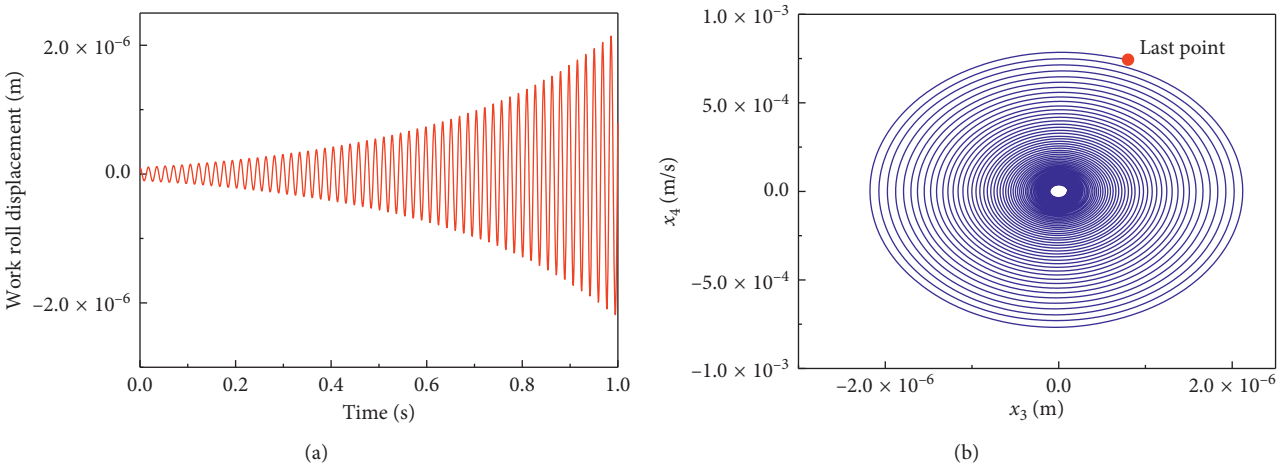

Figure 9: Dynamic response of the work roll displacement and the phase diagram under $\mu^* = 0.0420$: (a) time history of work roll displacement; (b) phase diagram.

Based on equation (12), the tension variation at the entry position (dT_b) and exit position (dT_f) is smaller compared with low friction coefficient rolling condition, so the fluctuation of the response rolling force ΔP_i increases, and the stability of the stand decreases. Meanwhile, when the friction is quite small, $\partial P/\partial h_{\text{out}}$ will increase with the decrease of friction coefficient; $F_{4,3}$ in equation (29) decreases, so the instantaneous dynamic structure spring constant decreases, and the fluctuation of the response rolling force ΔP_i caused by the strip exit thickness variation will increase, so the stability of the stand is decreased.

4.3. Stable Range Analysis of Other Rolling Parameters

4.3.1. Calculation of Limited Rolling Speed. Based on this coupled vertical-horizontal-torsional vibration analysis model, rolling speed has been chosen as the Hopf bifurcation parameter to obtain the limited stability rolling speed of the UCM tandem cold rolling mill, and other rolling conditions are shown in Table 1. The actual bifurcation point of rolling speed is 25.1 m/s. Figure 10 shows the time history of work roll displacement under the rolling speed of 25.2 m/s. According to Figure 10, the displacement amplitude of the work roll shows a divergence trend, and the self-excited vibration happens. The critical rolling speed calculated by the proposed chatter model is 25.1 m/s.

Figure 11 shows the tension and roll gap variation in No. 4 and No. 5 stands obtained from the Production Data Acquisition (PDA) system. As is shown in Figure 11(b), when the rolling speed is 22.1 m/s, the back and front tension of the No. 5 stand fluctuate within a small range and the mill stand is stable. However, when the rolling speed is raised to 23.0 m/s, the back and front tension of the No. 5 stand fluctuate more violently, and the front tension of the No. 5 stand begins to diverge as shown in Figure 11(a). It is found that the roll gap of No. 4 and No. 5 stands fluctuates more violently by comparing Figures 11(c) and 11(d). Meanwhile,

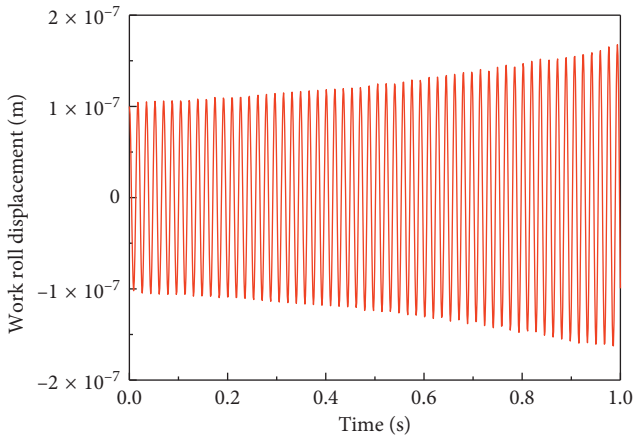

Figure 10: Work roll time history displacement under the rolling speed of 25.2 m/s.

a sudden and harsh vibration noise will be heard in the No. 5 stand, and finally the strip breaks. It shows mill chatter appears under the speed of 23.0 m/s, and the actual critical rolling speed is 23.0 m/s.

The calculated critical rolling speed is 25.1 m/s, while the actual critical rolling speed is 23.0 m/s. There is a certain relative error between the calculated critical speed and actual critical rolling speed. This is due to the small coefficient difference in Jacobian matrix. With the change of rolling speed, the actual value of the tension and friction is changed. And the calculated value of tension factor n_t and friction coefficient in $\partial P/\partial h$ and $\partial M/\partial h$ is a little different with the actual value. So, the calculated limited rolling speed is a little bigger than the actual value. However, by comparing the critical rolling speed calculated by the proposed model with the actual critical rolling speed, it can be seen that the proposed model is still accurate.

The vibration is largely influenced by the friction coefficient and rolling speed. Based on equation (13), Figure 12 shows the friction coefficient response of No. 5 stand versus speed. Despite the changes of speed, the friction coefficient is still in the stability range of 0.0048–0.0401. It is divided into two regions. In region 1, both the friction coefficient and rolling speed are in the stable range. In region 2, the friction coefficient is still in the stable range, while the speed exceeds the limited speed range. When the rolling speed is lower than 25.1 m/s, the mill system is stable without changing the lubrication conditions. And when the rolling speed is higher than 25.1 m/s, the stand is unstable. However, the friction coefficient is in the middle value of stable range under the speed is 25.1 m/s, so mill chatter might be eliminated by reducing the basic friction coefficient (by improving the lubrication characteristics, such as increasing the concentration of emulsion, increasing spray flow, and improving the property of the base oil).

4.3.2. Calculation of Maximum Reduction. Assuming the entry thickness is constant, the exit thickness is variable. And the exit thickness has been chosen as the Hopf bifurcation parameter. Other calculated rolling conditions are shown in Table 1. Then, the calculated bifurcation point of exit thickness is 0.168 mm. The optimal setting range of reduction for No. 5 stand is 0–44%. When the reduction of No. 5 stand is 44%, the increase of reduction leads to a lower mill stand stability. The reason is also related to the increase of rolling force variation under the larger reduction rolling conditions.

As can be seen in Table 1, in normal rolling schedule, the reduction rate is 33.3%. And the max reduction is up to 44%. In reality, considering there are other factors that influence the stand stability, such as rolling speed, and lubrication conditions, the max reduction is lower than 44%. In general, the effect of the reduction in the mill stability is lower than the improvement of friction coefficient.

4.3.3. Front Tension Stable Range. When the work roll velocity is 22.1 m/s, the calculated bifurcation point of exit tension is 1.5–133 MPa. Small front tension means that the rolling force will be quite large. So, under the same excitation interferences, the variation of rolling force will be much bigger, and the stand stability is decreased. When the front tension is big enough, tension factor n_t decreases, leading to a larger value in $\partial P/\partial h$ and $\partial M/\partial h$. As a result, the fluctuation of rolling force and roll torque increases, and the stability of the system is reduced as well. So, the influence of tension on the mill stability is smaller than other parameters.

These results can be used to estimate mill chatter in a certain stand. And the stable range of friction, reduction, and tension can be used to adjust the rolling schedule in the UCM mill to avoid mill chatter under high rolling speed.

5. Conclusion

(1) A new multiple degrees of freedom and nonlinear dynamic vertical-horizontal-torsional coupled mill chatter model for UCM cold rolling mill is established. In the dynamic rolling process model, the time-varying coupling effect between rolling force, roll torque variation, and fluctuation of strip thickness and tension is formulated. In the vibration model, the movement of work roll in both vertical-horizontal-torsional directions and the multiroll characteristics in the UCM rolling mill are considered. Finally, the dynamic relationship of roll movement responses and dynamic changes in the roll gap is formulated.

(2) Selecting the friction coefficient as the Hopf bifurcation parameter and by using Routh–Hurwitz determinant, the Hopf bifurcation point of the mill vibration system is calculated, and the bifurcation characteristics are analyzed. Research shows that either too low or too high friction coefficient increases the probability of mill chatter. When the friction coefficient is extremely low, the mill system produces a stable limit cycle. With the friction continuing to increase, the phase trajectory will converge toward the origin point. However, the limit cycle of phase diagram disappears and disperses outward under high friction rolling conditions.

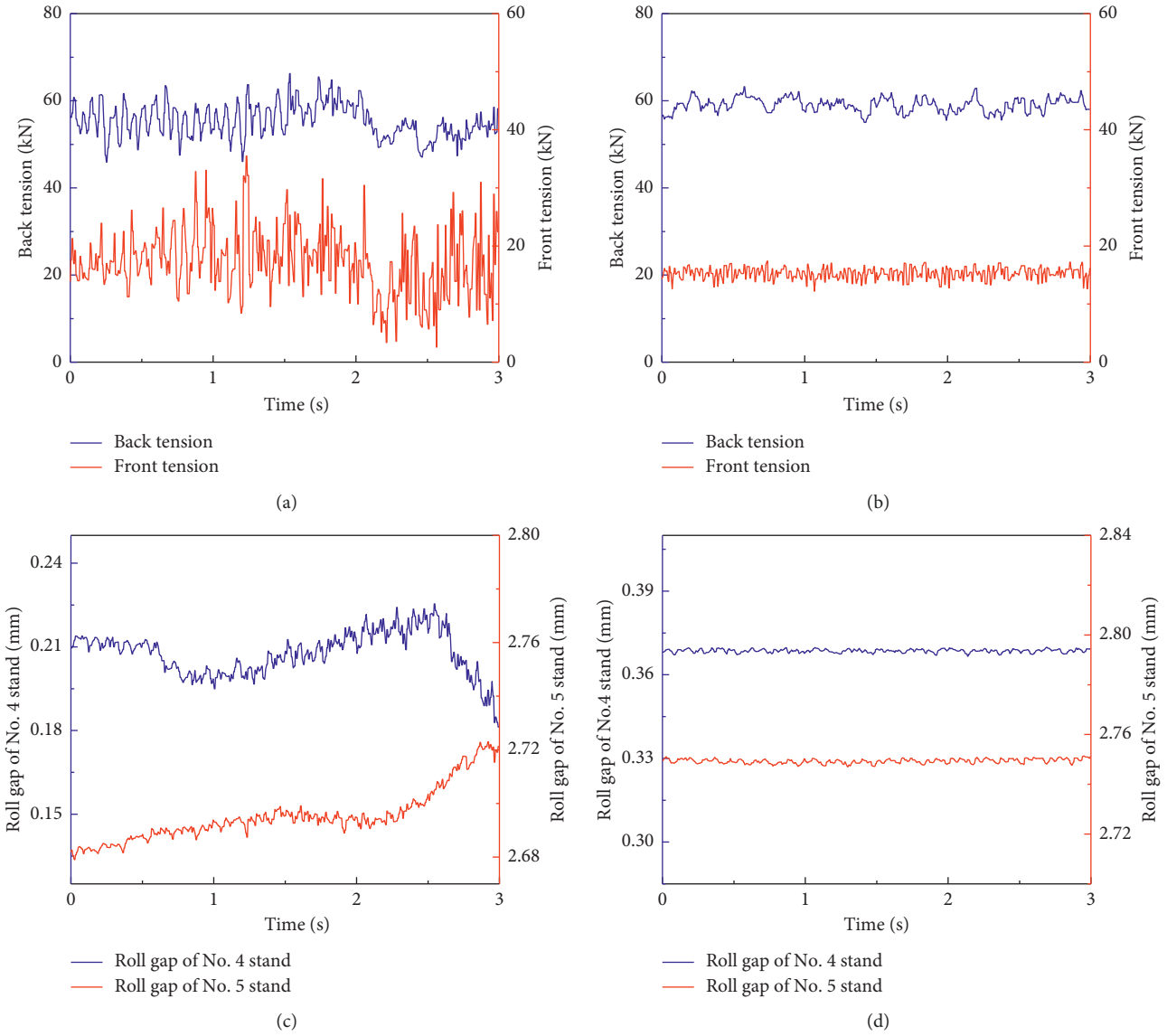

Figure 11: Tension and roll gap time history: (a) back and front tension of No. 5 stand under the speed of 23.0 m/s; (b) back and front tension of No. 5 stand under the speed of 22.1 m/s; (c) roll gap of No. 4 and No. 5 stands under the speed of 23.0 m/s; (d) roll gap of No. 4 and No. 5 stands under the speed of 22.1 m/s.

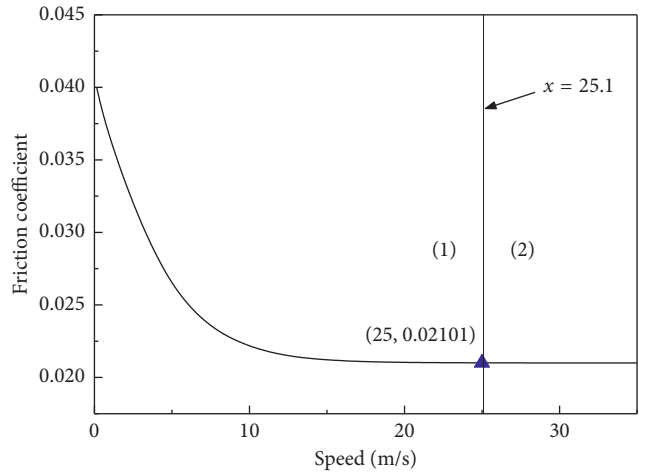

Figure 12: Friction coefficient response of No. 5 stand versus speed.

(3) Based on the coupled mill chatter model, the mill system's stable limited rolling speed, stable range of reduction, and front tension are investigated. Without changing the rolling speed, the most effective way to eliminate mill chatter is to change the lubrication conditions and adjust the reduction schedule. And the effect of tension on the vibration is quite limited. These methods can be used to improve the chatter phenomena in rolling mill under high rolling speed. The proposed vibration model can also be used to design an optimum rolling schedule in the UCM tandem cold rolling mill and to determine the appearance of mill chatter under certain rolling conditions.

Data Availability

The rolling conditions data used to support the findings of this study are included within the article.

Conflicts of Interest

The authors declare that they have no conflicts of interest regarding the publication of this manuscript.

Acknowledgments

This work was supported by the National Natural Science Foundation of China (51774084 and 51634002), the National Key R&D Program of China (2017YFB0304100), the Fundamental Research Funds for the Central Universities (N170708020), and the Open Research Fund from the State Key Laboratory of Rolling and Automation, Northeastern University (2017RALKFKT006).

References

[1] I. S. Yun, W. R. D. Wilson, and K. F. Ehmann, "Review of chatter studies in cold rolling," *International Journal of Machine Tools and Manufacture*, vol. 38, no. 12, pp. 1499–1530, 1998.

[2] I.-S. Yun, W. R. D. Wilson, and K. F. Ehmann, "Chatter in the strip rolling process, Part 1: dynamic model of rolling," *Journal of Manufacturing Science and Engineering*, vol. 120, no. 2, pp. 330–336, 1998.

[3] J. Tlusty, G. Chandra, S. Critchley, and D. Paton, "Chatter in cold rolling," *CIRP Annals*, vol. 31, no. 1, pp. 195–199, 1982.

[4] N. M. Reza, F. M. Reza, M. Salimi, and H. Shojaei, "Experimental investigations and ALE finite element method analysis of chatter in cold strip rolling," *ISIJ International*, vol. 52, no. 12, pp. 2245–2253, 2012.

[5] M. R. Niroomand, M. R. Forouzan, M. Salimi, and H. Shojaei, "Experimental investigations and ALE finite element method analysis of chatter in cold strip rolling," *ISIJ International*, vol. 52, no. 12, pp. 2245–2253, 2012.

[6] M. R. Niroomand, M. R. Forouzan, and M. Salimi, "Theoretical and experimental analysis of chatter in tandem cold rolling mills based on wave propagation theory," *ISIJ International*, vol. 55, no. 3, pp. 637–646, 2015.

[7] S. Kapil, P. Eberhard, and S. K. Dwivedy, "Nonlinear dynamic analysis of a parametrically excited cold rolling mill," *Journal of Manufacturing Science and Engineering*, vol. 136, no. 4, p. 041012, 2014.

[8] Y. Kimura, Y. Sodani, N. Nishiura, N. Ikeuchi, and Y. Mihara, "Analysis of chaffer in tandem cold rolling mills," *ISIJ International*, vol. 43, no. 1, pp. 77–84, 2003.

[9] N. Fujita, Y. Kimura, K. Kobayashi et al., "Dynamic control of lubrication characteristics in high speed tandem cold rolling," *Journal of Materials Processing Technology*, vol. 229, pp. 407–416, 2016.

[10] A. Heidari and M. R. Forouzan, "Optimization of cold rolling process parameters in order to increasing rolling speed limited by chatter vibrations," *Journal of Advanced Research*, vol. 4, no. 1, pp. 27–34, 2013.

[11] A. Heidari, M. R. Forouzan, and S. Akbarzadeh, "Effect of friction on tandem cold rolling mills chattering," *ISIJ International*, vol. 54, no. 10, pp. 2349–2356, 2014.

[12] A. Heidari, M. R. Forouzan, and S. Akbarzadeh, "Development of a rolling chatter model considering unsteady lubrication," *ISIJ International*, vol. 54, no. 1, pp. 165–170, 2014.

[13] A. Heidari, M. R. Forouzan, and M. R. Niroomand, "Development and evaluation of friction models for chatter simulation in cold strip rolling," *International Journal of Advanced Manufacturing Technology*, vol. 96, no. 4, pp. 1–21, 2018.

[14] Y. Kim, C.-W. Kim, S. Lee, and H. Park, "Dynamic modeling and numerical analysis of a cold rolling mill," *International Journal of Precision Engineering and Manufacturing*, vol. 14, no. 3, pp. 407–413, 2013.

[15] P. V. Krot, "Nonlinear vibrations and backlashes diagnostics in the rolling mills drive trains," in *Proceedings of the 6th EUROMECH Nonlinear Dynamics Conference*, Saint Petersburg, Russia, July 2008.

[16] S. Liu, B. Sun, S. Zhao, J. Li, and W. Zhang, "Strongly nonlinear dynamics of torsional vibration for rolling mill's electromechanical coupling system," *Steel Research International*, vol. 86, no. 9, pp. 984–992, 2015.

[17] S. Liu, J. Wang, J. Liu, and Y. Li, "Nonlinear parametrically excited vibration and active control of gear pair system with time-varying characteristic," *Chinese Physics B*, vol. 24, no. 10, pp. 303–311, 2015.

[18] B. D. Hassard, N. D. Kazarinoff, and Y. H. Wan, *Theory and Applications of Hopf Bifurcation*, Cambridge University Press, Cambridge, UK, 1981.

[19] B. H. K. Lee, S. J. Price, and Y. S. Wong, "Nonlinear aeroelastic analysis of airfoils: bifurcation and chaos," *Progress in Aerospace Sciences*, vol. 35, no. 3, pp. 205–334, 1999.

[20] K. Nishimura, T. Ikeda, and Y. Harata, "Localization phenomena in torsional rotating shaft systems with multiple centrifugal pendulum vibration absorbers," *Nonlinear Dynamics*, vol. 83, no. 3, pp. 1705–1726, 2015.

[21] T. Zhang and H. Dai, "Bifurcation analysis of high-speed railway wheel-set," *Nonlinear Dynamics*, vol. 83, no. 3, pp. 1511–1528, 2015.

[22] Z. Y. Gao, Y. Zang, and T. Han, "Hopf bifurcation and stability analysis on the mill drive system," *Applied Mechanics & Materials*, vol. 121-126, pp. 1514–1520, 2012.

[23] L. Zeng, Y. Zang, and Z. Gao, "Hopf bifurcation control for rolling mill multiple-mode-coupling vibration under nonlinear friction," *Journal of Vibration and Acoustics*, vol. 139, no. 6, article 061015, 2017.

[24] S. Liu, Z. Wang, J. Wang, and H. Li, "Sliding bifurcation research of a horizontal-torsional coupled main drive system of rolling mill," *Nonlinear Dynamics*, vol. 83, pp. 441–455, 2015.

[25] Y. Peng, M. Zhang, J.-L. Sun, and Y. Zhang, "Experimental and numerical investigation on the roll system swing vibration characteristics of a hot rolling mill," *ISIJ International*, vol. 57, no. 9, pp. 1567–1576, 2017.
[26] J. Pittner and M. A. Simaan, "Optimal control of continuous tandem cold metal rolling," in *Proceedings of 2008 American Control Conference*, Seattle, WA, USA, June 2008.
[27] R. B. Sims and D. F. S. Arthur, "Speed dependent variables in cold strip rolling," *Journal of Iron and Steel Institute*, vol. 172, no. 3, pp. 285–295, 1952.
[28] S. Z. Chen, D. H. Zhang, J. Sun, J. S. Wang, and J. Song, "Online calculation model of rolling force for cold rolling mill based on numerical integration," in *Proceedings of the 24th Chinese Control and Decision Conference (CCDC)*, Taiyuan, China, May 2012.
[29] D. R. Bland and H. Ford, "The calculation of roll force and torque in cold strip rolling with tensions," *Proceedings of the Institution of Mechanical Engineers*, vol. 159, no. 1, pp. 144–163, 2006.
[30] R. Hill, "Relations between roll-force, torque, and the applied tensions in strip-rolling," *Proceedings of the Institution of Mechanical Engineers*, vol. 163, no. 1, pp. 135–140, 2006.
[31] R. E. Johnson and Q. Qi, "Chatter dynamics in sheet rolling," *International Journal of Mechanical Sciences*, vol. 36, no. 7, pp. 617–630, 1994.
[32] Z. Gao, L. Bai, and Q. Li, "Research on critical rolling speed of self-excited vibration in the tandem rolling process of thin strip," *Journal of Mechanical Engineering*, vol. 53, no. 12, pp. 118–132, 2017.
[33] R. C. Dorf and R. H. Bishop, *Modern Control Systems*, University of California, Davis, CA, USA, 12th edition, 2010.
[34] W. M. Liu, "Criterion of hopf bifurcations without using eigenvalues," *Journal of Mathematical Analysis and Applications*, vol. 182, no. 1, pp. 250–256, 1994.
[35] L. Zeng, Y. Zang, and Z. Gao, "Multiple-modal-coupling modeling and stability analysis of cold rolling mill vibration," *Shock and Vibration*, vol. 2016, Article ID 2347386, 26 pages, 2016.